Journal of Power Sources 549 (2022) 232111

Contents lists available at ScienceDirect

Journal of Power Sources

journal homepage: www.elsevier.com/locate/jpowsour

Dodecahedral carbon with hierarchical porous channels and bi-heteroatom modulated interface for high-performance symmetric supercapacitors

Jieru Yang [a], Jian Meng [a], Leiqian Zhang [a], Kaibin Chu [a,b], Wei Zong [c], Lingfeng Ge [d], Siyu Fu [a], Jiale Ge [a], Haiyan Zhu [a], Guanjie He [e], Dan J.L. Brett [e], Feili Lai [b,*], Tianxi Liu [a,**]

[a] Key Laboratory of Synthetic and Biological Colloids, Ministry of Education, School of Chemical and Material Engineering, International Joint Research Laboratory for Nano Energy Composites, Jiangnan University, Wuxi, 214122, PR China
[b] Department of Chemistry, KU Leuven, Celestijnenlaan 200F, Leuven, 3001, Belgium
[c] Christopher Ingold Laboratory, Department of Chemistry, University College London, 20 Gordon Street, London, WC1H 0AJ, UK
[d] School of Chemistry, University of Bristol, Cantock's Close, Bristol, BS8 1TS, UK
[e] Department of Chemical Engineering, University College London, London, WC1E 7JE, UK

HIGHLIGHTS

- B, N co-doped, hierarchical porous carbon is obtained by pyrolyzing ZIF-8 with H_3BO_3.
- COMSOL Multiphysics and DFT jointly illustrate the improved storage performance.
- B, N co-doped strategy shows a synergistic effect on improving the adsorption of H^+.
- A hierarchical porous structure facilitates the penetration of electrolytes.

GRAPHICAL ABSTRACT

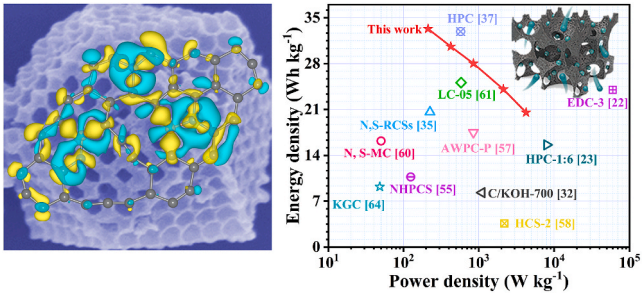

ARTICLE INFO

Keywords:
Hierarchical porous carbon
Dual-doped
Supercapacitors
COMSOL Multiphysics simulation
DFT calculation

ABSTRACT

Hierarchical porous channels and a well-modulated interface are two main parameters for electrode materials that can promote their energy storage performance by accelerating the electrolyte diffusion and realizing their strong coupling with electrolyte ions. Inspired by the COMSOL Multiphysics simulations and density functional theory calculations, we design B, N dual-doped, hierarchical porous carbon (BN-HPC) by pyrolyzing hierarchical porous zeolitic imidazolate framework-8 with boric acid. The resulted BN-HPC electrode achieves a high specific capacitance of 236.9 F g^{-1} at a current density of 1 A g^{-1} in 1 M H_2SO_4 electrolyte, which is further assembled into the BN-HPC//BN-HPC symmetric supercapacitor with a high energy density of 33.3 Wh kg^{-1} at a power density of 212.5 W kg^{-1}. The excellent energy storage performance of the BN-HPC electrode is attributed to its hierarchical porous structure and bi-heteroatom (N and B) doped carbon surface with a low binding energy value of −2.77 eV. This work provides a general and fresh insight into the design of dodecahedral carbon by combining hierarchical porous structure and bi-heteroatom doping strategy that can be used for not only aqueous supercapacitors but also other energy storage devices.

* Corresponding author.
** Corresponding author.
E-mail addresses: feili.lai@kuleuven.be (F. Lai), txliu@jiangnan.edu.cn (T. Liu).

https://doi.org/10.1016/j.jpowsour.2022.232111
Received 23 June 2022; Received in revised form 16 August 2022; Accepted 7 September 2022
Available online 24 September 2022

1. Introduction

Nowadays, environmental pollution and energy shortage have prompted the explorations of high-performance energy storage technologies [1–5], among which supercapacitors have attracted much more attention because of their fast charge-discharge rate, excellent power density, and long lifespan [6–8]. Depending on the different mechanisms of charge storage, supercapacitors can be divided into two categories, namely electrochemical double layer capacitors (EDLCs) and pseudocapacitors [9–11]. Metal oxides [12–15] and conducting polymers [16–21] are generally used materials for the electrodes of pseudocapacitors. Compared with conductive polymers and metal oxides, carbon-based materials are widely used as electrodes for supercapacitors with EDLC mechanism due to their low processing cost, high specific surface area, and excellent electrical conductivity. The ideal carbon materials should have large specific surface areas and tunable pore structures (including macropores, mesopores, and micropores). In particular, the macropores, mesopores, and micropores in carbon materials play different roles in the storage of electrolyte ions, the diffusion/penetration of electrolyte, and the adsorption of electrolyte ions, respectively [22,23]. Therefore, it becomes a feasible strategy to prepare novel carbon materials with well-designed and hierarchical porous structures that can allow the effective penetration of electrolyte, improve the utilization of specific surface area, and shorten the ion diffusion pathway, leading to enhanced electrochemical energy storage performance of carbon electrodes. In recent years, a great deal of work has been reported on synthetic strategies for hierarchical porous carbons [24–27], such as three-dimensional B and N codoped core-shell carbon nanofibers [25], polyvinyl chloride-derived nitrogen-doped hierarchically porous carbon nanosheets [26]. Among precursors for carbon materials, metal-organic framework (MOF)-derived carbons are regarded as promising candidates for energy storage due to their controlled porosities, large specific surface area, and diverse geometries [9,28,29].

Apart from the hierarchical porous structures of MOF-derived carbons, it is also an effective method to improve their energy storage performance by introducing ideal heteroatoms (*e.g.,* B [30,31], N [32,33], P [34], S [35], F [36], and O [37]) into the carbon skeletons [38]. In particular, the heteroatoms of B and N show more similar atomic radii and chemical properties to those of C, probably leading to a high content of doped-heteroatom in the carbon lattice. As a typical MOF, zeolitic imidazolate frameworks (ZIFs) not only have the advantages of large pore capacity and high specific surface but also contain abundant imidazolium groups as nitrogen self-doping materials [39] that can distribute the N heteroatoms in the carbon matrix efficiently and uniformly. For instance, R. R. Salunkhe and co-workers prepared the nanoporous carbon materials successfully by using ZIF-8 as a precursor for supercapacitor electrode materials with a maximum specific capacitance of 8.36 F cm^{-3} (19.0 F g^{-1}) [40]. More importantly, it has also been demonstrated to boost the electrochemical energy storage performance of monoheteroatom-doped carbons by introducing two different heteroatomic dopants with a synergistic effect [41,42]. However, it is still difficult to realize uniform doping of bi-heteroatoms in hierarchical porous carbons due to the limitations of synthetic techniques.

In this study, a novel strategy was developed by pyrolyzing hierarchical porous zeolitic imidazolate framework-8 with boric acid to obtain the B, N dual-doped, hierarchical porous carbon (BN-HPC) that shows a high specific surface area of 852 m^2 g^{-1} and modulated carbon surface for coupling electrolyte ions. It was found that the resulted BN-HPC electrode has a large capacitance of 236.9 F g^{-1} at a current density of 1 A g^{-1} in 1 M H_2SO_4. The as-assembled BN-HPC//BN-HPC symmetric supercapacitor shows not only a high energy density of 33.3 Wh kg^{-1} at a power density of 212.5 W kg^{-1}, but also high capacitance retention of 78% at a current density of 10 A g^{-1} after 2500 cycles.

2. Experimental section

2.1. Materials

Zinc nitrate hexahydrate ($Zn(NO_3)_2{\cdot}6H_2O$), 2-methylimidazole, boric acid (H_3BO_3), carbon black, tetrahydrofuran (THF), methanol, ammonia, N-methylpyrrolidone (NMP), polyvinylidene difluoride (PVDF), and sulfuric acid (H_2SO_4) were supplied by Sinopharm Chemical Reagent Co., Ltd and used as received. The polystyrene was prepared as reported previously [32]. The deionized water (18 MΩ cm^{-2}) was from the ultra-pure purification system.

2.2. Synthesis of single-crystal ordered macroporous ZIF-8

The single-crystal ordered macroporous ZIF-8 (SOM ZIF-8) was synthesized *via* impregnation method and double-solvent-assisted method as shown in Fig. S2 [43]. The as-prepared ordered polystyrene (PS) microspheres were used as the template, soaked in 135 mL methanol solution containing 2-methylimidazole (20.25 g) and $Zn(NO_3)_2{\cdot}6H_2O$ (24.45 g) for 1 h, and then vacuumed for 30 min. Subsequently, the impregnated PS template was withdrawn and dried at 60 °C for several hours, which was further immersed in a mixed solution of ammonia and CH_3OH (1:2 v/v) for 24 h to obtain the PS@ZIF-8 by filtering and drying for 12 h. The PS template in PS@ZIF-8 was removed by immersing the PS@ZIF-8 in THF solvent for 24 h. Finally, the obtained SOM ZIF-8 was dried at 110 °C for 24 h to remove the residual THF.

2.3. Synthesis of ZIF-8

$Zn(NO_3)_2{\cdot}6H_2O$ (1.28 g) and 2-methylimidazole (4.86 g) were dissolved in 50 mL methanol separately, which were mixed rapidly and kept for 24 h. The as-formed white powder of ZIF-8 was collected by centrifugation, washed with methanol several times, and dried at 60 °C overnight.

2.4. Synthesis of N-doped hierarchical porous carbon and N-doped porous carbon

The dried SOM ZIF-8 was carbonized at 900 °C for 1 h under Ar atmosphere to obtain N-doped hierarchical porous carbon (N-HPC). Additionally, ZIF-8 was carbonized to prepare N-doped porous carbon (N-PC) as a contrast sample.

2.5. Synthesis of B, N dual-doped, hierarchical porous carbon

N-HPC and H_3BO_3 were mixed and transferred in a ceramic boat, which was carbonized at 900 °C for 1 h under Ar atmosphere to generate B, N dual-doped, hierarchical porous carbon (BN-HPC).

2.6. Characterization

The morphologies of various samples were investigated *via* transmission electron microscopy (TEM, JEM-2100plus, Japan), scanning electron microscopy (SEM, HITACHIS4800, Japan), and the elemental distribution on the sample was scanned by energy-dispersive X-ray spectroscopy (EDS). The powder patterns of various samples were recorded on an X-ray diffractometer (XRD, Bruker D8, Germany) with Cu Kα radiation (λ = 1.5418 Å). X-ray photoelectron spectroscopy (XPS, Axis supra, British) was performed to analyze the compositions of samples. The specific surface area and the pore size distribution were gained by the Brunauer-Emmett-Teller (BET) method and density functional theory (DFT) model.

2.7. Electrochemical measurements

The working electrode was fabricated by mixing 80 wt% of active material, 10 wt% of carbon black and 10 wt% of polyvinylidene difluoride (PVDF) binder, to obtain a homogeneous paste using a certain amount of NMP. The mixture was loaded onto carbon paper with a mass loading of ~1.5 mg cm^{-2}. For a three-electrode system, the cyclic voltammetry (CV) measurement, galvanostatic charge-discharge (GCD), and electrochemical impedance spectra (EIS) were tested in 1 M H_2SO_4 electrolyte. A graphite electrode and an Ag/AgCl electrode were used as the counter and reference electrodes, respectively. For a two-electrode system, two symmetrical working electrodes were fabricated in a test device composed of a separator (filter paper), electrolyte (1 M H_2SO_4), and two electrodes.

The mass-based specific capacitance (C_s, F g^{-1}) measured on a three-electrode system was calculated from the galvanostatic charge-discharge curves using the following equation:

$$C_s = \frac{I\Delta t}{mV} \quad (1)$$

The symmetric supercapacitor devices were constructed using two electrodes with the same loading amount of electroactive materials. The C_s can be calculated from the galvanostatic charge-discharge curves according to the following equation:

$$C_s = \frac{I \times \Delta t}{2m \times V} \quad (2)$$

where I (A) is the current, Δt (s) is the discharge time, m (g) is the mass of single electroactive material, and V (V) is the potential.

The energy density E (Wh kg^{-1}) and power density P (W kg^{-1}) are calculated according to the following equations:

$$E = \frac{1}{2} \times C \times V^2 \quad (3)$$

$$P = \frac{E}{\Delta t} \quad (4)$$

3. Result and discussion

The advantages of hierarchical porous carbon for electrolyte diffusion/penetration of electrolyte in the electrode were firstly confirmed by COMSOL Multiphysics simulations. Here, we constructed two ideal models of porous and solid dodecahedra that simulated hierarchical porous and solid carbons (Fig. 1a), respectively. In detail, the free space inside the hierarchical porous carbon can be quickly and fully occupied by the electrolyte within 4 ms, while the diffusion of the electrolyte would be blocked outside the solid carbon completely. By taking the central points of two carbons as examples, the electrolyte concentration in the central point of hierarchical porous carbon approach to the high level of the outside electrolyte (t = 4 ms) as compared to the low electrolyte concentration (~0, t = 4 ms) in the central point of solid carbon (Fig. 1b). Additionally, the electrolyte penetrations at the ektexines of two carbon models were also investigated in Fig. 1c, where the

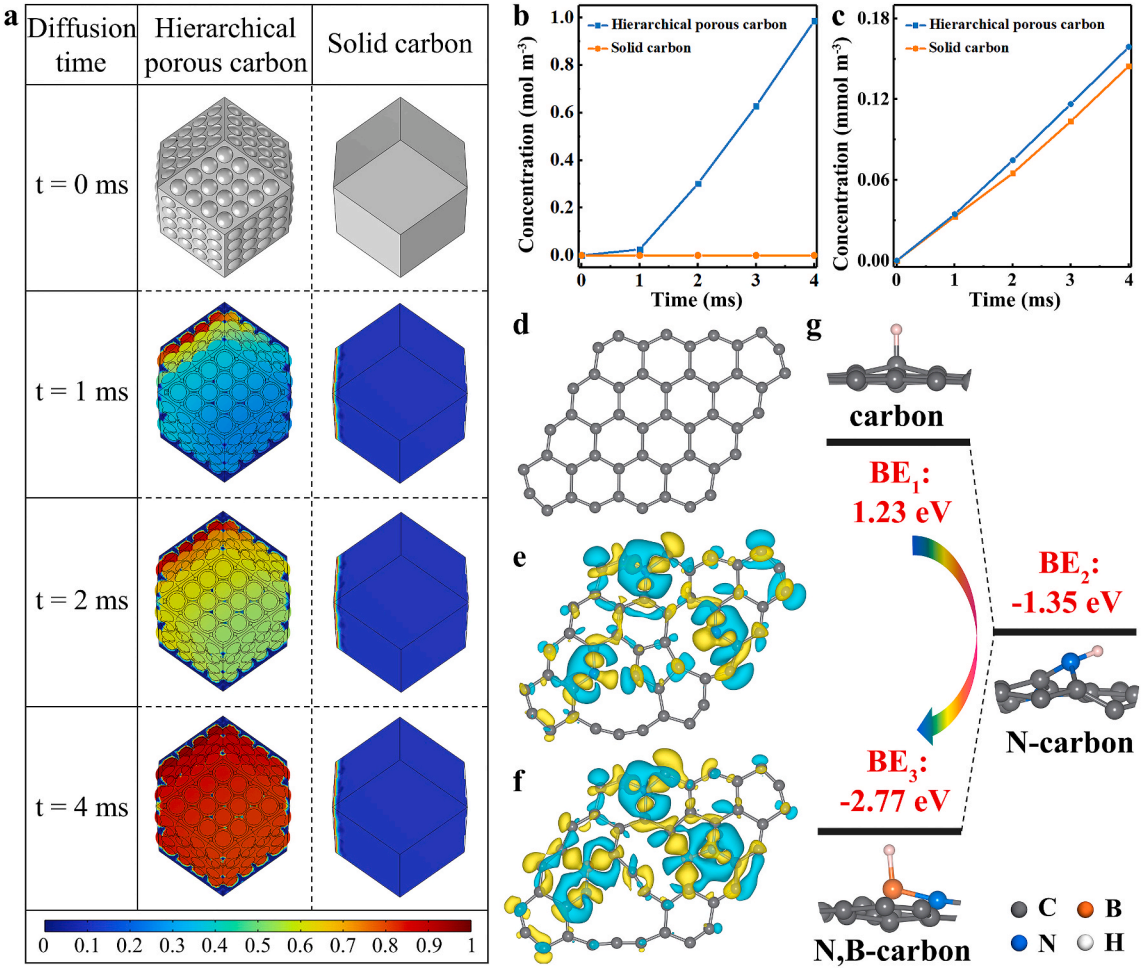

Fig. 1. (a) The concentration of electrolyte in two models of hierarchical porous carbon and solid carbon at different diffusion times. The electrolyte concentrations at (b) the central points and (c) the ektexines in the two models of hierarchical porous carbon and solid carbon. (d) The optimized structure of carbon. The partial charge densities of (e) N-carbon and (f) N, B-carbon. (g) The binding energy values of hydrogen atoms on various models of carbon, N-carbon, and N, B-carbon.

hierarchical porous carbon displays a slightly higher concentration than that of solid carbon. It is because the electrolyte can penetrate into the ektexine of hierarchical porous carbon from abundant sides. Therefore, the COMSOL simulations demonstrate it is necessary to construct hierarchical porous carbons, which is beneficial for the diffusion/penetration of electrolyte during the electrochemical process.

From another perspective of interface chemistry, density functional theory (DFT) calculation was also conducted to observe the interfacial environment between the B, N dual-doped carbon and proton in the acid electrolyte during the electrochemical energy storage process. After doping nitrogen in the carbon model (Fig. 1d), the delocalized charges in the N-carbon model are mainly located near the N dopants (Fig. 1e), indicating its enhanced electrochemical activity for coupling the protons. The further doped B heteroatom in the N, B-carbon model can intensify the charge distribution (Fig. 1f) with more active sites as compared to the N-carbon model. According to the calculated binding energy (BE) values between the protons and various carbon models in Fig. 1g and Fig. S1, the optimized BE values on carbon (BE_1), N-carbon (BE_2), N, B-carbon (BE_3), and B-carbon (BE_4) models are equal to be 1.23, −1.35, −2.77, and 1.21 eV, respectively. It indicates the synergistic effect of N and B dual-doping in improving the adsorption of protons. Therefore, it can significantly improve the electrochemical property of carbon materials by combining hierarchical porous and B, N dual-doped structures into carbon materials.

Based on the above theoretical calculations, we designed and synthesized B, N dual-doped, hierarchical porous carbon (BN-HPC) with detailed processes illustrated in Fig. 2a and Fig. S2, where the polystyrene (PS) microspheres with a uniform size of ~170 nm (Fig. S3) and boric acid (H_3BO_3) were used as the template for the formation of hierarchical porous structure [43–47] and the resource for the generation of doped boron atoms in BN-HPC (more details can be referred in the Supporting Information), respectively. As the scanning electron microscopy (SEM) images of BN-HPC are shown in Fig. 2b–d, the BN-HPC keeps the framework of ZIF-8 well and displays a typical rhombic dodecahedron shape, which contains abundant and uniform macropores with the average size of ~188 nm. We also prepared a contrast sample of nitrogen-doped porous carbon (N-PC) without a PS template, which exhibits the solid and blocked structure (Fig. S4b). Energy dispersive spectrum (EDS) elemental mappings of BN-HPC (Fig. 2e) demonstrate the presence of C, N, and B elements with uniform distributions of doped heteroatoms (nitrogen and boron) on its surface. To be noted, the BN-HPC maintains a similar morphology as compared to the nitrogen-doped hierarchical porous carbon (N-HPC, Fig. S5), demonstrating the negative effect of the boron-doping process on the structural stability of BN-HPC. The microstructural and morphological differences between BN-HPC and N-PC were investigated by transmission electron microscopy (TEM). As shown in Fig. S6 and Fig. S7, the BN-HPC reveals a hierarchical porous structure compared with the N-PC.

The crystal structures of BN-HPC and its contrast samples were analyzed by the X-ray diffraction (XRD) technique. As shown in Fig. 3a, all of the BN-HPC, N-HPC, and N-PC show similar XRD patterns with two distinct characteristic board peaks at approximately $2\theta = 24^\circ$ and 43°, which correspond to the (002) and (100) planes of graphitic carbon [48]. The X-ray photoelectron spectroscopy (XPS) analysis was used to identify the surface components of the BN-HPC (Fig. 3b–e), N-PC (Fig. S8), and N-HPC (Fig. S9). The XPS survey spectrum shown in Fig. 3b confirms the existence of B, N, and C elements in the BN-HPC, which corresponds with the above EDS elemental mappings (Fig. 2e) well. As shown in Fig. 3c, the C 1s XPS spectrum of BN-HPC shows three peaks at 284.7, 285.5, and 288.7 eV, corresponding to sp^2C, C═N/C–O, and C–N, respectively [49]. The high-resolution XPS spectrum of the N 1s peak (Fig. 3d) confirms the presence of pyridinic N (398.0 eV), pyrrolic N (399.3 eV), and graphitic N (402.5 eV) in the BN-HPC [50]. The high-resolution XPS spectrum of the B 1s (Fig. 3e) can be deconvoluted into B–N (190.4 eV) and B–O (191.5 eV) species [49]. Additionally, the contents of B and N were calculated to be 6% and 16%, respectively. The specific surface area and pore structure of BN-HPC were determined by investigating its nitrogen adsorption-desorption isotherm (Fig. 3f). From the inset in Fig. 3f, it can be observed that the content of mesopore in BN-HPC is higher than that of N-PC, demonstrating the successful formation of the abundant mesoporous structure by using the strategy in this work [9]. As a result, the BN-HPC shows a higher specific surface area of 852 $m^2\ g^{-1}$ on the basis of the Brunauer-Emmett-Teller (BET) method than that of 248 $m^2\ g^{-1}$ of N-PC without using the PS template.

The electrochemical performance of N-PC, N-HPC, and BN-HPC for supercapacitors was firstly evaluated in a three-electrode system by using 1 M H_2SO_4 aqueous solution as the electrolyte. As the cyclic voltammetry (CV) curves (scan rate: 100 mV s^{-1}) of N-PC, N-HPC, and BN-HPC shown in Fig. 4a, the BN-HPC displays the largest enclosed area and implies its largest specific capacitance among three samples, resulting from the promoted reaction kinetics by doping bi-heteroatoms and accelerated electron/ion transport behaviors by constructing hierarchical porous structure. The galvanostatic charge-discharge (GCD) curves (Fig. 4b) at a current density of 1 A g^{-1} are approximately symmetrical and quasitriangular, which indicate the capacitive behaviors of the BN-HPC, N-HPC, and N-PC. From the GCD curves, the specific capacitance of BN-HPC is calculated to be 236.9 F g^{-1} at a current density of 1 A g^{-1}, which is much higher than those of N-PC (152.2 F g^{-1}) and N-HPC (221.8 F g^{-1}). The excellent electrochemical performance of BN-HPC has resulted from the synergistic effect of the hierarchical porous structure and doped bi-heteroatoms (N and B). The hierarchical porous structure is beneficial for shortening the ion

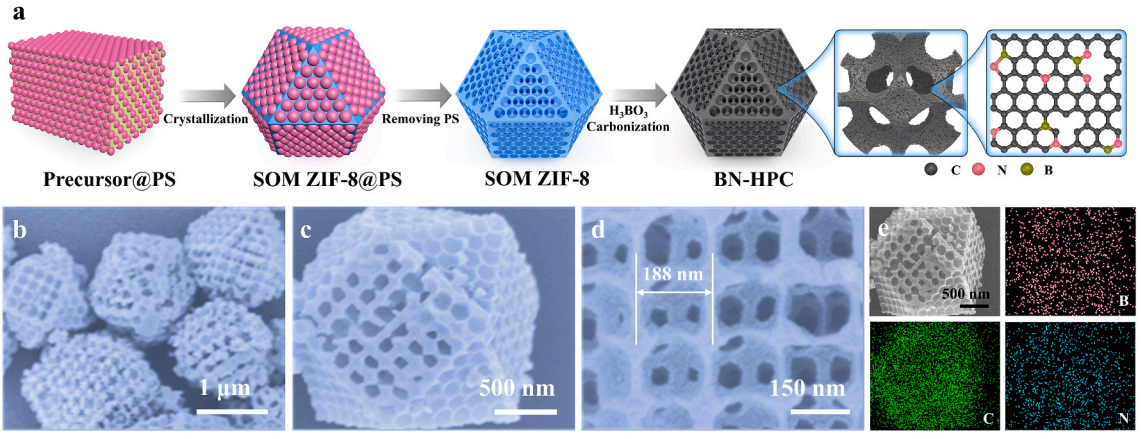

Fig. 2. (a) Schematic illustration for the synthesis of BN-HPC. (b–d) SEM images of BN-HPC at different magnifications. (e) SEM image of BN-HPC and its corresponding EDS elemental mappings of B, C, and N.

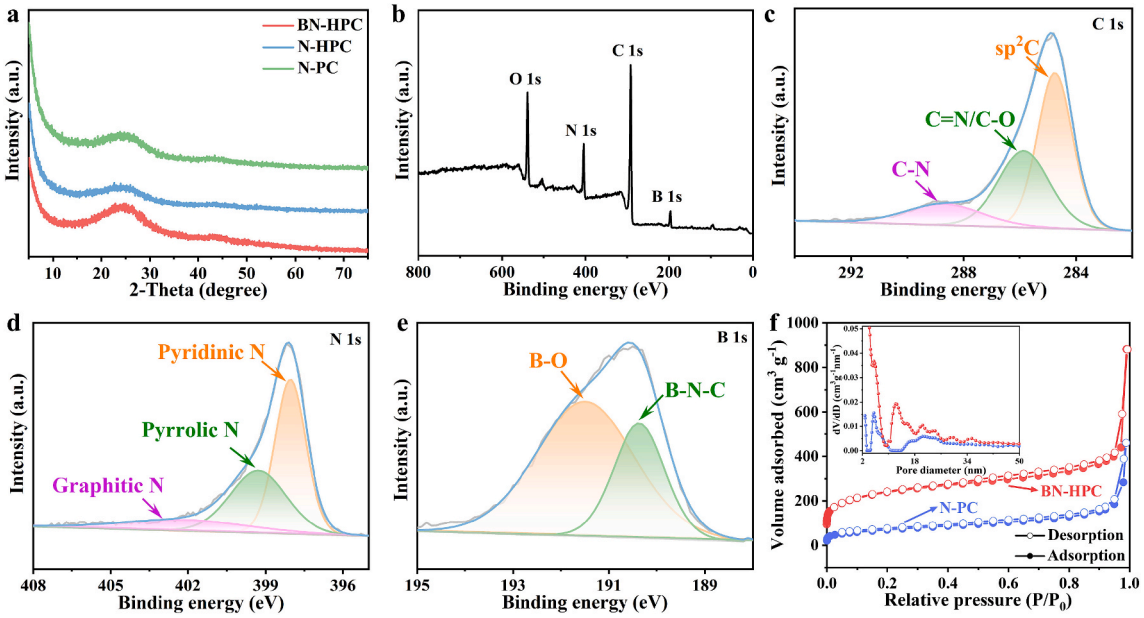

Fig. 3. (a) XRD patterns of BN-HPC, N-HPC, and N-PC. (b) XPS survey spectrum of BN-HPC. High-resolution XPS spectra for (c) C 1s, (d) N 1s, and (e) B 1s of BN-HPC. (f) N_2 adsorption-desorption isotherms of BN-HPC and N-PC (inset is the corresponding pore size distributions of BN-HPC and N-PC).

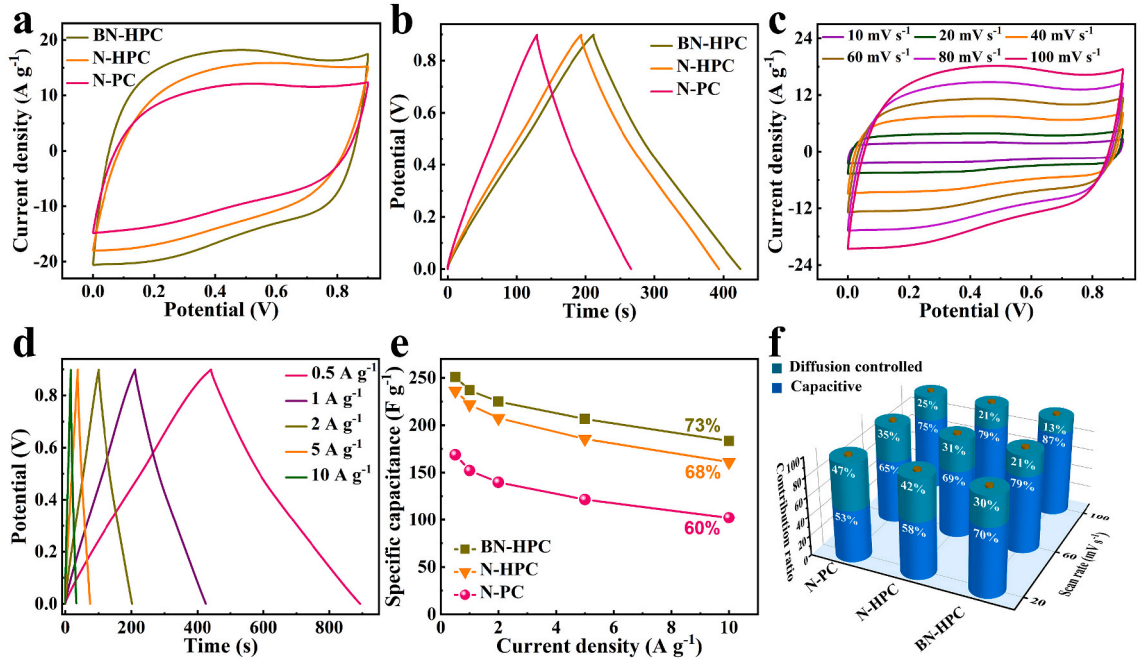

Fig. 4. (a) CV curves at a scan rate of 100 mV s^{-1} and (b) GCD profiles at a current density of 1 A g^{-1} of N-PC, N-HPC, and BN-HPC. (c) CV curves under different scan rates and (d) GCD curves under different current densities of BN-HPC. (e) Specific capacitances of N-PC, N-HPC, and BN-HPC at different current densities from 0.5 to 10 A g^{-1}. (f) Capacitive contributions of N-PC, N-HPC, and BN-HPC at different scan rates.

transport pathway for efficient contact between the electrode material and the electrolyte, which matches well with the COMSOL simulations (Fig. 1a–c). On the other hand, the doped N and B atoms in the hierarchical porous carbon skeleton could further modulate the interfacial wettability of the electrode and enhance the adsorption of electrolyte ions on its surface with detailed discussion in the DFT calculations (Fig. 1d–g).

The electrochemical properties of BN-HPC were further investigated by CV curves under different scan rates (Fig. 4c) and GCD profiles under different current densities (Fig. 4d), which can maintain the shapes well even at a high scan rate/current density and indicate the excellent rate stability of BN-HPC electrode. As shown in Fig. 4e, the specific capacitances of BN-HPC, N-HPC, and N-PC decrease with the increase of current density from 0.5 to 10 A g^{-1}. Among them, the BN-HPC shows the highest capacitance retention of 73% than those of N-HPC (68%) and N-PC (60%). To evaluate the electrochemical conductivity and ion diffusion capability of BN-HPC, N-PC, and N-HPC, the electrochemical impedance spectra (EIS) tests were carried out and shown in Fig. S10. The equivalent series resistances acquired from the curve intercept at the real axis are 2.8 Ω (BN-HPC), 6.8 Ω (N-HPC), and 12.1 Ω (N-PC), respectively. The steeper vertical line of BN-HPC than those of N-PC and N-HPC implies lower electron transfer resistance and low ion diffusion of

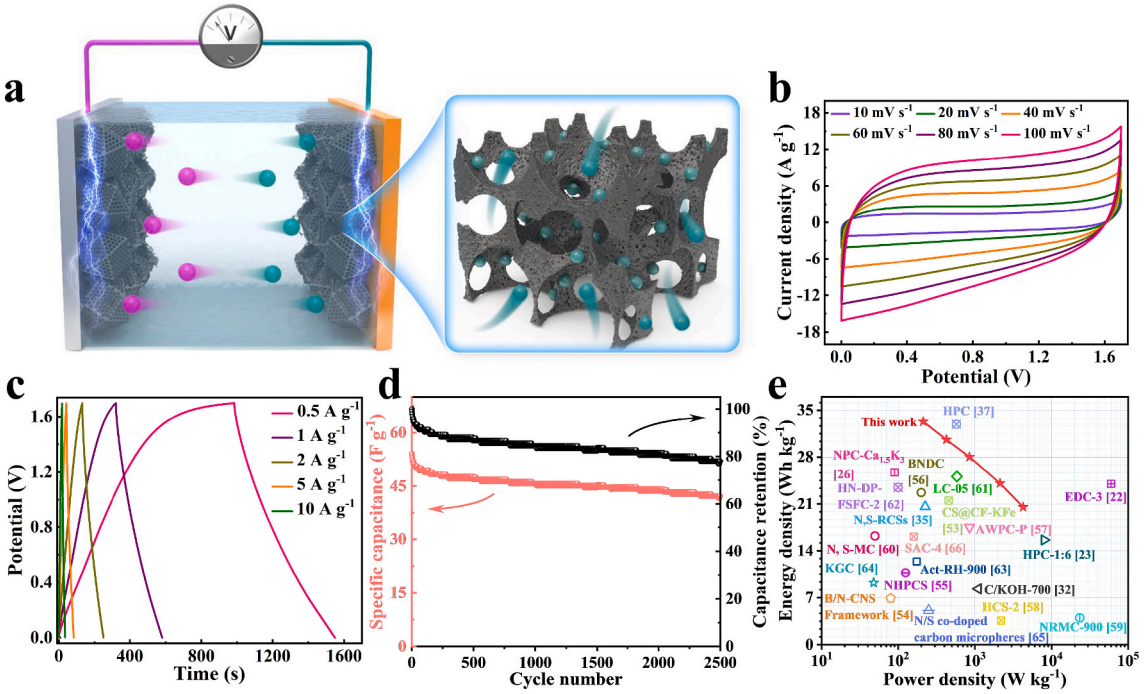

Fig. 5. (a) The diagram for the energy storage mechanism in a symmetric supercapacitor by using B, N dual-doped hierarchical porous carbon. The electrochemical performance of the as-assembled symmetric system: (b) CV curves at various scan rates, (c) GCD profiles under different current densities, (d) cycling stability at a current density of 10 A g^{-1}, and (e) Ragone plots of BN-HPC//BN-HPC symmetric supercapacitor.

the BN-HPC electrode [51]. In particular, the capacitive (k_1v) and diffusion ($k_2v^{1/2}$) contributions can be determined quantitatively at a given scan rate according to the equation: $i/v^{1/2} = k_1v^{1/2} + k_2$. Here, the capacitive and diffusion controls represent the ultrarapid reaction kinetics of ion adsorption/desorption and sluggish reaction kinetics of the chemical adsorption, respectively. As shown in Fig. 4f, the BN-HPC electrode reveals the highest capacitive contribution at any scan rates (70% at a scan rate of 20 mV s^{-1}) than those of N-HPC (58%) and N-PC (53%), which originates from the doped bi-heteroatoms (N and B) in the BN-HPC with ultrarapid reaction kinetics for H^+ adsorption/desorption process [52].

To evaluate the electrochemical performance of the BN-HPC electrode under realistic application conditions, the BN-HPC//BN-HPC symmetric supercapacitor was assembled and shown in Fig. 5a. The electrochemical properties of the BN-HPC were discussed by CV with different scan rates (Fig. 5b) and GCD with various current densities (Fig. 5c). The CV and GCD curves keep the shapes without obvious distortion even at a high scanning rate (100 mV s^{-1}) and a high current density (10 A g^{-1}), implying the excellent rate stability of the symmetric supercapacitor. In particular, the device displays the capacitance of 83 F g^{-1} at 0.5 A g^{-1} with the remaining capacitance of 51.2 F g^{-1} at 10 A g^{-1}. As shown in Fig. 5d and Table S1, the BN-HPC//BN-HPC symmetric supercapacitor still maintains capacitance retention of 78% at a high current density of 10 A g^{-1} after 2500 cycles, indicating its potential for practical applications. As shown in Fig. 5e and Table S2, the Ragone plots of the BN-HPC//BN-HPC symmetric supercapacitor reveals a high energy density of 33.3 Wh kg^{-1} at a power density of 212.5 W kg^{-1}, which shows a comparable property with previously reported materials, such as N/S co-doped carbon microspheres (5.1 Wh kg^{-1} at 250 W kg^{-1}), N-doped porous carbon nanosheets (25.7 Wh kg^{-1} at 90 W kg^{-1}), hollow carbon spheres (3.6 Wh kg^{-1} at 2200 W kg^{-1}) and so on [22,23,26,32,35,37,53–66].

4. Conclusion

In conclusion, B, N dual-doped, hierarchical porous carbon (BN-HPC) was well prepared under the guidance of COMSOL Multiphysics simulation and density functional theory calculations. A series of electrochemical measurements were conducted and proved the enhanced energy storage performance of the BN-HPC electrode (236.9 F g^{-1} at 1 A g^{-1}) due to its hierarchical porous structure and bi-heteroatom (N and B) doped carbon surface. By using BN-HPC, we assembled the BN-HPC//BN-HPC symmetric supercapacitor and delivered a high energy density of 33.3 Wh kg^{-1} at a power density of 212.5 W kg^{-1} for further practical applications. In spite of the comparable energy storage performance of BN-HPC electrode with others, we provided a general and fresh thought into the design of dodecahedral carbon by combining hierarchical porous structure and bi-heteroatom doping strategy from both experimental and theoretical perspectives, which has important significance to guide the future design of other carbon materials for supercapacitors.

CRediT authorship contribution statement

Jieru Yang: Investiagation, Writing-original draft. **Jian Meng:** Formal analysis. **Leiqian Zhang:** Data curation. **Kaibin Chu:** Data curation. **Wei Zong:** Data curation. **Lingfeng Ge:** Data curation. **Siyu Fu:** Visualization. **Jiale Ge:** Visualization. **Haiyan Zhu:** Data interpretation. **Guanjie He:** Writing-review & editing. **Dan J.L. Brett:** Writing-review & editing. **Feili Lai:** Methodology, Supervision, Writing-review & editing. **Tianxi Liu:** Supervision, Writing-review & editing, Funding acquisition.

Declaration of competing interest

The authors declare that they have no known competing financial interests or personal relationships that could have appeared to influence the work reported in this paper.

Data availability

Data will be made available on request.

Acknowledgments

This work was supported by the National Natural Science Foundation of China (52161135302, 21674019), the Research Foundation Flanders (G0F2322N), Shanghai Scientific and Technological Innovation Project (18JC1410600), and the Program of the Shanghai Academic Research Leader (17XD1400100). We also thank the characterizations supported by the Central Laboratory, School of Chemical and Material Engineering, Jiangnan University.

Appendix A. Supplementary data

Supplementary data to this article can be found online at https://doi.org/10.1016/j.jpowsour.2022.232111.

References

[1] W. Zong, Y. Ouyang, Y.-E. Miao, T. Liu, F. Lai, Recent advances and perspectives of 3D printed micro-supercapacitors: from design to smart integrated devices, Chem. Commun. 58 (2022) 2075–2095, https://doi.org/10.1039/d1cc05544e.
[2] K. Subhani, X. Jin, P. Mahon, A. Lau, N. Salim, Graphene aerogel modified carbon fiber reinforced composite structural supercapacitors, Compos. Commun. 24 (2021), 100663, https://doi.org/10.1016/j.coco.2021.100663.
[3] Z. Wang, G. Qu, C. Wang, X. Zhang, G. Xiang, P. Hou, et al., Modified Co_4N by B-doping for high-performance hybrid supercapacitors, Nanoscale 12 (2020) 18400–18408, https://doi.org/10.1039/d0nr04043f.
[4] Y. Zhou, S. Xu, J. Yang, Z. Zhou, S. Peng, X. Wang, et al., A thin carbon nanofiber/branched carbon nanofiber nanocomposite for high-performance supercapacitors, New J. Chem. 46 (2022) 3091–3094, https://doi.org/10.1039/d1nj06171b.
[5] W. Zong, H. Guo, Y. Ouyang, L. Mo, C. Zhou, G. Chao, et al., Topochemistry-driven synthesis of transition-metal selenides with weakened van der Waals force to enable 3D-printed Na-ion hybrid capacitors, Adv. Funct. Mater. 32 (2022), 2110016, https://doi.org/10.1002/adfm.202110016.
[6] K. Jayaramulu, D. Dubal, B. Nagar, V. Ranc, O. Tomanec, M. Petr, et al., Ultrathin hierarchical porous carbon nanosheets for high-performance supercapacitors and redox electrolyte energy storage, Adv. Mater. 30 (2018), 1705789, https://doi.org/10.1002/adma.201705789.
[7] S. Yuan, W. Fan, D. Wang, L. Zhang, Y.-E. Miao, F. Lai, et al., 3D printed carbon aerogel microlattices for customizable supercapacitors with high areal capacitance, J. Mater. Chem. A 9 (2021) 423–432, https://doi.org/10.1039/d0ta08750e.
[8] F. Lai, J. Feng, T. Heil, Z. Tian, J. Schmidt, G.-C. Wang, et al., Partially delocalized charge in Fe-doped $NiCo_2S_4$ nanosheet-mesoporous carbon-composites for high-voltage supercapacitors, J. Mater. Chem. A 7 (2019) 19342–19347, https://doi.org/10.1039/c9ta06250e.
[9] Y. Wang, M. Qiao, X. Mamat, Nitrogen-doped macro-meso-micro hierarchical ordered porous carbon derived from ZIF-8 for boosting supercapacitor performance, Appl. Surf. Sci. 540 (2021), 148352, https://doi.org/10.1016/j.apsusc.2020.148352.
[10] X. Luo, S. Chen, T. Hu, Y. Chen, F. Li, Renewable biomass-derived carbons for electrochemical capacitor applications, SusMat 1 (2021) 211–240, https://doi.org/10.1002/sus2.8.
[11] F. Lai, Y. Huang, Y.-E. Miao, T. Liu, Controllable preparation of multi-dimensional hybrid materials of nickel-cobalt layered double hydroxide nanorods/nanosheets on electrospun carbon nanofibers for high-performance supercapacitors, Electrochim. Acta 174 (2015) 456–463, https://doi.org/10.1016/j.electacta.2015.06.031.
[12] S. Pawar, D. Patil, D. Nandi, M. Islam, T. Sakurai, S.-H. Kim, et al., Cobalt-based metal oxide coated with ultrathin ALD-MoS_2 as an electrode material for supercapacitors, Chem. Eng. J. 435 (2022), 135066, https://doi.org/10.1016/j.cej.2022.135066.
[13] Y. Liu, X. Xu, Z. Shao, S. Jiang, Metal-organic frameworks derived porous carbon, metal oxides and metal sulfides-based compounds for supercapacitors application, Energy Storage Mater. 26 (2020) 1–22, https://doi.org/10.1016/j.ensm.2019.12.019.
[14] L. Lyu, W. Antink, Y. Kim, C. Kim, T. Hyeon, Y. Piao, Recent development of flexible and stretchable supercapacitors using transition metal compounds as electrode materials, Small 17 (2021), 2101974, https://doi.org/10.1002/smll.202101974.
[15] F. Lai, C. Yang, R. Lian, K. Chu, J. Qin, W. Zong, et al., Three-phase boundary in cross-coupled micro-mesoporous networks enabling 3D-printed and ionogel-based quasi-solid-state micro-supercapacitors, Adv. Mater. 32 (2020), 2002474, https://doi.org/10.1002/adma.202002474.
[16] Q. Meng, K. Cai, Y. Chen, L. Chen, Research progress on conducting polymer based supercapacitor electrode materials, Nano Energy 36 (2017) 268–285, https://doi.org/10.1016/j.nanoen.2017.04.040.
[17] Y. Huang, H. Li, Z. Wang, M. Zhu, Z. Pei, Q. Xue, et al., Nanostructured Polypyrrole as a flexible electrode material of supercapacitor, Nano Energy 22 (2016) 422–438, https://doi.org/10.1016/j.nanoen.2016.02.047.
[18] I. Marriam, Y. Wang, M. Tebyetekerwa, Polyindole batteries and supercapacitors, Energy Storage Mater. 33 (2020) 336–359, https://doi.org/10.1016/j.ensm.2020.08.010.
[19] G. Qu, J. Cheng, X. Li, D. Yuan, P. Chen, X. Chen, et al., A fiber supercapacitor with high energy density based on hollow graphene/conducting polymer fiber electrode, Adv. Mater. 28 (2016) 3646–3652, https://doi.org/10.1002/adma.201600689.
[20] H. Wang, Z. Yu, M. El-Kady, M. Anderson, M. Kowal, M. Li, et al., Graphene/oligoaniline based supercapacitors: towards conducting polymer materials with high rate charge storage, Energy Storage Mater. 19 (2019) 137–147, https://doi.org/10.1016/j.ensm.2019.02.019.
[21] S. Liu, K. Wan, C. Zhang, T. Liu, Polyaniline-decorated 3D carbon porous network with excellent electrolyte wettability and high energy density for supercapacitors, Compos. Commun. 24 (2021), 100610, https://doi.org/10.1016/j.coco.2020.100610.
[22] W. Yu, H. Wang, S. Liu, N. Mao, X. Liu, J. Shi, et al., N, O-codoped hierarchical porous carbons derived from algae for high-capacity supercapacitors and battery anodes, J. Mater. Chem. A 4 (2016) 5973–5983, https://doi.org/10.1039/c6ta01821a.
[23] X. Lei, F. Pan, C. Hua, S. Wang, B. Xiong, Y. Liu, et al., Oxide-doped hierarchically porous carbon for high-performance supercapacitor, J. Alloys Compd. 901 (2022), 163624, https://doi.org/10.1016/j.jallcom.2022.163624.
[24] S. Dutta, A. Bhaumik, K.C.-W. Wu, Hierarchically porous carbon derived from polymers and biomass: effect of interconnected pores on energy applications, Energy Environ. Sci. 7 (2014) 3574–3592, https://doi.org/10.1039/c4ee01075b.
[25] B. Dahal, S.-H. Chae, A. Muthurasu, T. Mukhiya, J. Gautam, K. Chhetri, et al., An innovative synthetic approach for core-shell multiscale hierarchically porous boron and nitrogen codoped carbon nanofibers for the oxygen reduction reaction, J. Power Sources 453 (2020), 227883, https://doi.org/10.1016/j.jpowsour.2020.227883.
[26] Z. Sheng, X. Lin, H. Wei, Y. Zhang, Z. Tian, C. Wang, et al., Green synthesis of nitrogen-doped hierarchical porous carbon nanosheets derived from polyvinyl chloride towards high-performance supercapacitor, J. Power Sources 515 (2021), 230629, https://doi.org/10.1016/j.jpowsour.2021.230629.
[27] A. Modak, A. Bhaumik, Porous carbon derived via KOH activation of a hypercrosslinked porous organic polymer for efficient CO_2, CH_4, H_2 adsorptions and high CO_2/N_2 selectivity, J. Solid State Chem. 232 (2015) 157–162, https://doi.org/10.1016/j.jssc.2015.09.022.
[28] D.-G. Wang, Z. Liang, S. Gao, C. Qu, R. Zou, Metal-organic framework-based materials for hybrid supercapacitor application, Coord. Chem. Rev. 404 (2020), 213093, https://doi.org/10.1016/j.ccr.2019.213093.
[29] G. Cai, P. Yan, L. Zhang, H.-C. Zhou, H.-L. Jiang, Metal-organic framework-based hierarchically porous materials: synthesis and applications, Chem. Rev. 121 (2021) 12278–12326, https://doi.org/10.1021/acs.chemrev.1c00243.
[30] Y.-B. Huang, P. Pachfule, J.-K. Sun, Q. Xu, From covalent-organic frameworks to hierarchically porous B-doped carbons: a molten-salt approach, J. Mater. Chem. A 4 (2016) 4273–4279, https://doi.org/10.1039/c5ta10170k.
[31] Y. Li, J. Huang, L. Kang, Z. Tian, F. Lai, D.J.L. Brett, et al., Self-assembled carbon nanoribbons with the heteroatom doping used as ultrafast charging cathodes in zinc-ion hybrid supercapacitors, Sci. China Mater. 65 (2022) 1495–1502, https://doi.org/10.1007/s40843-021-1923-6.
[32] F. Gao, J. Qu, C. Geng, G. Shao, M. Wu, Self-templating synthesis of nitrogen-decorated hierarchical porous carbon from shrimp shell for supercapacitors, J. Mater. Chem. A 4 (2016) 7445–7452, https://doi.org/10.1039/c6ta01314g.
[33] Z. Tian, F. Lai, T. Heil, S. Cao, M. Autonietti, Synthesis of carbon frameworks with N, O and S-lined pores from gallic acid and thiourea for superior CO_2 adsorption and supercapacitors, Sci. China Mater. 63 (2020) 748–757, https://doi.org/10.1007/s40843-019-1254-9.
[34] X. Luo, Q. Yang, Y. Dong, X. Huang, D. Kong, B. Wang, et al., Maximizing pore and heteroatom utilization within N,P-co-doped polypyrrole-derived carbon nanotubes for high-performance supercapacitors, J. Mater. Chem. A 8 (2020) 17558–17567, https://doi.org/10.1039/d0ta06238c.
[35] F. Lai, G. Zhou, F. Li, Z. He, D. Yong, W. Bai, et al., Highly dual-heteroatom-doped ultrathin carbon nanosheets with expanded interlayer distance for efficient energy storage, ACS Sustain. Chem. Eng. 6 (2018) 3143–3153, https://doi.org/10.1021/acssuschemeng.7b03161.
[36] J. Zhou, L. Xu, L. Li, X. Li, Polytetrafluoroethylene-assisted N/F co-doped hierarchically porous carbon as a high performance electrode for supercapacitors, J. Colloid Interface Sci. 545 (2019) 25–34, https://doi.org/10.1016/j.jcis.2019.03.010.
[37] X. Qian, L. Miao, J. Jiang, G. Ping, W. Xiong, Y. Lv, et al., Hydrangea-like N/O codoped porous carbons for high-energy supercapacitors, Chem. Eng. J. 388 (2020), 124208, https://doi.org/10.1016/j.cej.2020.124208.
[38] M. Wu, S. Tong, L. Jiang, B. Hou, X. Li, Y. Zhang, et al., Nitrogen-doped porous carbon composite with three-dimensional conducting network for high rate supercapacitors, J. Alloys Compd. 844 (2020), 156217, https://doi.org/10.1016/j.jallcom.2020.156217.
[39] S. Zhang, J. Luo, F. Zhang, X. He, Highly porous and thermally stable zeolitic imidazolate framework-8/aramid nanofibers composite separator for lithium-ion batteries, Compos. Commun. 32 (2022), 101183, https://doi.org/10.1016/j.coco.2022.101183.
[40] R. Salunkhe, C. Young, J. Tang, T. Takei, Y. Ide, N. Kobayashi, et al., A high-performance supercapacitor cell based on ZIF-8-derived nanoporous carbon using an organic electrolyte, Chem. Commun. 52 (2016) 4764–4767, https://doi.org/10.1039/c6cc00413j.
[41] C. Nguyen, S. Lee, Y. Chung, W.-H. Chiang, K. Wu, Synergistic effect of metal-organic framework-derived boron and nitrogen heteroatom-doped three-dimensional porous carbons for precious-metal-free catalytic reduction of

nitroarenes, Appl. Catal. B Environ. 257 (2019), 117888, https://doi.org/10.1016/j.apcatb.2019.117888.
[42] W. Feng, N. Feng, W. Liu, Y. Cui, C. Chen, T. Dong, et al., Liquid-state templates for constructing B, N, co-doping porous carbons with a boosting of potassium-ion storage performance, Adv. Energy Mater. 11 (2020), 2003215, https://doi.org/10.1002/aenm.202003215.
[43] Z. Zhu, H. Yin, Y. Wang, C.-H. Chuang, L. Xing, M. Dong, et al., Coexisting single-atomic Fe and Ni sites on hierarchically ordered porous carbon as a highly efficient ORR electrocatalyst, Adv. Mater. 32 (2020), 2004670, https://doi.org/10.1002/adma.202004670.
[44] Q. Li, Z. Dai, J. Wu, W. Liu, T. Di, R. Jiang, et al., Fabrication of ordered macro-microporous single-crystalline MOF and its derivative carbon material for supercapacitor, Adv. Energy Mater. 10 (2020), 1903750, https://doi.org/10.1002/aenm.201903750.
[45] M. Qiao, Y. Wang, Q. Wang, G. Hu, X. Mamat, S. Zhang, et al., Hierarchically ordered porous carbon with atomically dispersed FeN_4 for ultra-efficient oxygen reduction reaction in PEMFC, Angew. Chem. Int. Ed. 59 (2020) 2688–2694, https://doi.org/10.1002/anie.201914123.
[46] Y.-R. Lv, X.-J. Zhai, S. Wang, H. Xu, R. Wang, S.-Q. Zang, 3D-ordered macroporous N-doped carbon encapsulating Fe-N alloy derived from a single-source metal-organic framework for superior oxygen reduction reaction, Chin. J. Catal. 42 (2021) 490–500, https://doi.org/10.1016/s1872-2067(20)63667-1.
[47] H. Hong, J. Liu, H. Huang, C. Etogo, X. Yang, B. Guan, et al., Ordered macro-microporous metal-organic framework single crystals and their derivatives for rechargeable aluminum-ion batteries, J. Am. Chem. Soc. 141 (2019) 14764–14771, https://doi.org/10.1021/jacs.9b06957.
[48] H. Lu, S. Liu, Y. Zhang, Y. Huang, C. Zhang, T. Liu, Nitrogen-doped carbon polyhedra nanopapers: an advanced binder-free electrode for high-performance supercapacitors, ACS Sustain. Chem. Eng. 7 (2019) 5240–5248, https://doi.org/10.1021/acssuschemeng.8b06159.
[49] R. Zhao, Q. Li, Z. Chen, V. Jose, X. Jiang, G. Fu, et al., B, N-doped ultrathin carbon nanosheet superstructure for high-performance oxygen reduction reaction in rechargeable zinc-air battery, Carbon 164 (2020) 398–406, https://doi.org/10.1016/j.carbon.2020.04.019.
[50] F. Lai, Y.-E. Miao, L. Zuo, H. Lu, Y. Huang, T. Liu, Biomass-derived nitrogen-doped carbon nanofiber network: a facile template for decoration of ultrathin nickel-cobalt layered double hydroxide nanosheets as high-performance asymmetric supercapacitor electrode, Small 12 (2016) 3235–3244, https://doi.org/10.1002/smll.201600412.
[51] L. Wan, E. Shamsaei, C. Easton, D. Yu, Y. Liang, X. Chen, et al., ZIF-8 derived nitrogen-doped porous carbon/carbon nanotube composite for high-performance supercapacitor, Carbon 121 (2017) 330–336, https://doi.org/10.1016/j.carbon.2017.06.017.
[52] Z. Ling, Z. Wang, M. Zhang, C. Yu, G. Wang, Y. Dong, et al., Sustainable synthesis and assembly of biomass-derived B/N co-doped carbon nanosheets with ultrahigh aspect ratio for high-performance supercapacitors, Adv. Funct. Mater. 26 (2016) 111–119, https://doi.org/10.1002/adfm.201504004.
[53] X. Zhang, H. Li, B. Qin, Q. Wang, X. Xing, D. Yang, et al., Direct synthesis of porous graphitic carbon sheets grafted on carbon fibers for high-performance supercapacitors, J. Mater. Chem. A 7 (2019) 3298–3306, https://doi.org/10.1039/c8ta11844b.
[54] J. Hao, J. Wang, S. Qin, D. Liu, Y. Li, W. Lei, B/N co-doped carbon nanosphere frameworks as high-performance electrodes for supercapacitors, J. Mater. Chem. A 6 (2018) 8053–8058, https://doi.org/10.1039/c8ta00683k.
[55] C. Wang, D. Wu, H. Wang, Z. Gao, F. Xu, K. Jiang, Biomass derived nitrogen-doped hierarchical porous carbon sheets for supercapacitors with high performance, J. Colloid Interface Sci. 523 (2018) 133–143, https://doi.org/10.1016/j.jcis.2018.03.009.
[56] Z. Zhao, Y. Xie, Electrochemical supercapacitor performance of boron and nitrogen co-doped porous carbon nanowires, J. Power Sources 400 (2018) 264–276, https://doi.org/10.1016/j.jpowsour.2018.08.032.
[57] C. Dai, J. Wan, J. Yang, S. Qu, T. Jin, F. Ma, et al., H_3PO_4 solution hydrothermal carbonization combined with KOH activation to prepare argy wormwood-based porous carbon for high-performance supercapacitors, Appl. Surf. Sci. 444 (2018) 105–117, https://doi.org/10.1016/j.apsusc.2018.02.261.
[58] X. Yang, Y. Li, P. Zhang, L. Sun, X. Ren, H. Mi, Hierarchical hollow carbon spheres: novel synthesis strategy, pore structure engineering and application for micro-supercapacitor, Carbon 157 (2020) 70–79, https://doi.org/10.1016/j.carbon.2019.10.008.
[59] F. Sun, J. Gao, X. Pi, L. Wang, Y. Yang, Z. Qu, et al., High performance aqueous supercapacitor based on highly nitrogen-doped carbon nanospheres with unimodal mesoporosity, J. Power Sources 337 (2017) 189–196, https://doi.org/10.1016/j.jpowsour.2016.10.086.
[60] Y. Lu, J. Liang, S. Deng, Q. He, S. Deng, Y. Hu, et al., Hypercrosslinked polymers enabled micropore-dominant N, S co-doped porous carbon for ultrafast electron/ion transport supercapacitors, Nano Energy 65 (2019), 103993, https://doi.org/10.1016/j.nanoen.2019.103993.
[61] W. Liu, Y. Yao, O. Fu, S. Jiang, Y. Fang, Y. Wei, et al., Lignin-derived carbon nanosheets for high-capacitance supercapacitors, RSC Adv. 7 (2017) 48537–48543, https://doi.org/10.1039/c7ra08531a.
[62] C. Chang, M. Li, H. Wang, S. Wang, X. Liu, H. Liu, et al., A novel fabrication strategy for doped hierarchical porous biomass-derived carbon with high microporosity for ultrahigh-capacitance supercapacitors, J. Mater. Chem. A 7 (2019) 19939–19949, https://doi.org/10.1039/c9ta06210f.
[63] C. Li, H. Chen, L. Zhang, S. Jiao, H. Zhang, J. Zhang, et al., Rice hull-derived carbon for supercapacitors: towards sustainable silicon-carbon supercapacitors, Polymers 13 (2021) 4463, https://doi.org/10.3390/polym13244463.
[64] X. Zhu, S. Yu, K. Xu, Y. Zhang, L. Zhang, G. Lou, et al., Sustainable activated carbons from dead ginkgo leaves for supercapacitor electrode active materials, Chem. Eng. Sci. 181 (2018) 36–45, https://doi.org/10.1016/j.ces.2018.02.004.
[65] H. Zhou, Y. Zhou, S. Wu, L. Li, Y. Li, M. Guo, et al., Synthesis of N/S co-doped porous carbon microspheres based on amino acid protic salt for supercapacitor, J. Alloys Compd. 829 (2020), 154549, https://doi.org/10.1016/j.jallcom.2020.154549.
[66] X.-L. Su, J.-R. Chen, G.-P. Zheng, J.-H. Yang, X.-X. Guan, P.Z. Liu, Xiu-Cheng, Three-dimensional porous activated carbon derived from loofah sponge biomass for supercapacitor applications, Appl. Surf. Sci. 436 (2018) 327–336, https://doi.org/10.1016/j.apsusc.2017.11.249.